Evaluation of nano/submicro pores in suspension plasma sprayed YSZ coatings

Yongli Zhao, Yan Wang, François Peyraut, Hanlin Liao, Ghislain Montavon, Marie-Pierre Planche, Jan Ilavsky, Audrey Lasalle, Alain Allimant

Evaluation of nano/submicro pores in suspension plasma sprayed YSZ coatings

Yongli Zhao [ab], Yan Wang [b*], François Peyraut [b], Hanlin Liao [b], Ghislain Montavon [b], Marie-Pierre Planche [b], Jan Ilavsky [c], Audrey Lasalle [d], Alain Allimant [d]

[a] School of Mechanical and Automotive Engineering, Shanghai University of Engineering Science, 201620, China

[b] ICB UMR 6303, CNRS, Université de Bourgogne Franche-Comté, UTBM, 90010 Belfort, France

[c] Advanced Photon Source, Argonne National Laboratory, 9700 S. Cass Avenue, Argonne, IL 60439, USA

[d] Saint-Gobain CREE, 84300 Cavaillon, France

*Corresponding author: E-mail: yan.wang@utbm.fr

Abstract:

Nano-submicro pores could considerably influence the coating performances and thus should be properly designed for the intended applications. However, it is challenging to characterize accurately such small pores in coatings. In this study, YSZ coatings were firstly manufactured by suspension plasma spray (SPS) and the nano-submicro pores in as-prepared coatings were investigated using Ultra-small-angle X-ray scattering (USAXS). Afterwards, a multivariate analysis on the effect of five different process parameters was carried out. The two main

results showed that: 1) the nano-submicro pores content in coatings has a negative correlation with suspension mass load and powder size, and a positive correlation with spray distance, spray step, and substrate surface roughness; 2) suspension mass load is the main factor affecting the content of nano-submicro pores. Then, a mathematical model for the prediction of nano-submicro pores was developed, and the control of nano-submicro pores content by using the predictive model was presented. Finally, the sintering effect on the evolution of nano-submicro pores was studied in-situ using USAXS as well.

Keywords: suspension plasma spray, nano-submicro pore, multivariate analysis, YSZ coating, predictive model, USAXS

1 Introduction

The coating properties strongly depend on the coating porosity, for example, porosity typically degrades the mechanical properties of coatings but improves their thermal insulation capabilities [1, 2]. However, in addition to the amount of porosity, the coating properties are also influenced by the nature of the individual pores, i.e., the size and the shape of pores as well as their relative proportions [2]. Thanks to the use of liquid carrier, suspension plasma spray (SPS) enables the manufacture of finely structured or nanostructured coatings. It has been proven that such structured coatings exhibit superior performances compared to the micrometer-sized coatings fabricated by conventional thermal spray technique [1]. SPS coatings contain a lot of submicrometric, and even nanometric, pores, playing an important

role in the coating performances. For example, smaller pores compared to larger pores lead to higher thermal resistance due to the penetration of the gas flow within the pores [3]. Therefore, the nano-submicro pores in the SPS coatings should be accurately characterized and properly designed for the intended applications.

Several methods are commonly implemented to quantify pores in coatings such as imaging method by analyzing SEM images of coating cross section [4], physical methods based on the intrusion of a liquid into the void network [2, 3], and electrochemical methods by analyzing the chemical reaction at the substrate/electrolyte interface [3]. But all these techniques are limited to the micrometer scale in a porous medium [5, 6]. To overcome the challenges in characterization of nano/submicro pores in SPS coatings, some new techniques were recently applied. Klement et al. [2] employed x-ray microscopy (XRM) to reconstruct a 3D imaging of pores and cracks at a resolution down to 50 nm. Nuclear magnetic resonance (NMR) cryoporometry was also used to characterize the SPS coating structure by determining porosity and pore size distribution at the range from 5 to 500 nm [7]. Here, the characterization was managed by Ultra-Small Angle X-ray Scattering (USAXS) because it is a non-destructive test without any limitation of resolution.

Due to phase transformations, grain growth and sintering occurring at elevated environment [8], the microstructure of coatings will change over time influencing by the way their initial performances. The traditional methods to study sintering effect are time-consuming, as they

require at first sintering the sample at high temperatures then taking it out from the high temperature environment, and finally cooling it before the observation. In the current study, in-situ observations of the sintering effect on the evolution of nano/submicro pores in SPS coatings were carried out by using the technique of USAXS.

As for conventional plasma spraying (APS), the microstructures of SPS coatings are typically tailored by controlling the spray conditions [4, 9]. However, SPS process is more complicated than APS hence it is more difficult to optimize the process parameters [10, 11]. Several researches have been already performed to investigate the relationship between the process parameters and the coating porosity. For example, Tesar [12] and Sokołowski [13] studied the influence of suspension formulation. Bacciochini et al [3] reported the effect of spray distance. Our previous work [9] confirmed that the coating porosity is linked to the substrate properties. However, those researches were focused on the influence of one or two process parameters at most. In order to facilitate the optimization of process parameters, it is highly desirable to study multiple parameters in the frame of a global view. In this study, YSZ coatings were manufactured by SPS technique with five different process parameters: suspension mass load, original powder size, spray distance, spray step, and substrate surface topology. A multivariate analysis was then carried out to reveal the influence trend and sensitivity of each process parameter. Finally, a mathematical model was developed in order to predict coating properties and to guide coating optimization for specific applications.

2 Experimental procedure

2.1 Coating manufacturing

YSZ powders with different particle sizes and different solid mass loads were dispersed in ethanol to prepare the suspensions. The YSZ particle size distributions are presented in Fig.1. DOLAPIX ET85 (Zschimmer & Schwarz, Germany) was added to reach the optimum suspension dispersion. The SPS coatings were deposited using the atmospheric plasma ProPlasma torch (Saint-Gobain Coating Solutions, Avignon, France). A twin-fluid atomizer developed with the Saint-Gobain company was used to inject the suspension into the plasma jet and was positioned 10 mm perpendicularly to the torch axis, and 6 mm downstream the anode face. Figure 2 shows the schematic of the SPS process and the twin-fluid atomizer. During the spray process, suspension was stored in a pressurized tank, under magnetic stirring to avoid sedimentation, and was delivered through the twin-fluid atomizer supplied with argon as atomizing gas. 304L stainless steel of 10 mm thickness and 25 mm diameter was used as substrate. Based on our previous work [9], where no obvious defects were observed in the interface region with a preheating temperature up to 300℃, similar spray conditions were used in this study. All substrates were therefore preheated before the spraying. The fixed process parameters are listed in Table 1, the variable process parameters and coating characteristics are summarized in Table 2.

2.2 Characterizations

Ultra-Small-Angle X-ray Scattering [14, 15] was used to analyze the nanometer to micrometer size pores of the SPS coatings. This technique can characterize the size distribution and volume fraction of pores in the sample under assumption of spherical pore shape. Samples were measured at 9ID-C USAXS/SAXS/WAXS instrument (Argonne National Laboratory, Argonne, IL, USA) [16].

Prior to the measurements, the coatings were detached from substrates by acid pickling in Aqua Regia (nitro-hydrochloric acid). The free-standing coatings were then cleaned with deionized water and ethanol and dried in environment subsequently. As-deposited samples (Table 2) were analyzed to reveal the relationship between manufacturing conditions and resulting porous structure. Further, in order to study the sintering effect on the pore size and volume evolution, selected samples were measured in-situ, using Linkam TS1500 furnace, at 1200 °C in air over 12 hours.

In-situ USAXS/SAXS/WAXS data collection consists of sequential runs of USAXS, SAXS, and WAXS devices, repeating whole cycle in approximately 4 minutes. The USAXS/SAXS/WAXS data were collected using 16.9 keV X-rays, beam size was 0.8 x 0.8mm for USAXS and 0.8 x 0.2 mm for SAXS and WAXS. Data included in this study are combined USAXS and SAXS data, spanning extended range of scattering vectors, q, from 10^{-4} to 1 $Å^{-1}$ [3, 17].

$$q = \frac{4\pi}{\lambda \ sin(\theta)} \qquad \text{Eq.1}$$

where λ is the wavelength of the X rays and 2θ is the scattering angle. WAXS data are not included in the present research (even though they were collected) as they did not bring in any new information.

Scattering data were reduced using data reduction programs Indra and Nika [16]. Data were placed on absolute intensity scale using standard instrument calibration methods. Size distribution of pores was analyzed using Irena package [18]. For scattering contrast of the pores the value of 1923.1 x 10^{20} [cm^{-4}] was retained. This is the scattering contrast between tetragonal YSZ and voids, calculated specifically for X-ray energy for 16.9 keV using Irena Scattering Contrast Calculator, which accounts for absorption edges of YSZ.

3 Results and discussions

3.1 Microstructure and nano/submicro pore analysis

Figure 3 shows the typical granular and porous microstructure of the as-prepared SPS coating [19, 20]. As reported by other researchers [2, 7], the pores in those SPS coating exhibit the same wide size range from nanometers up to several micrometers. Furthermore, the coating is mainly composed of flattened splats (F), spherical particles (S), and irregular particles (I) as indicated by the arrows in Fig 3. The splats are fully molten particles that spread while impacting onto the substrate. Those splats formed the denser layers of the coating containing small pores in the scale of nano-submicrometer. The spherical particles correspond to molten particles that solidify prior their impact. The irregular particles are identical to initial feedstock due to a no or partial melting probably. As a consequence, spherical and irregular particles lead to larger pores in coatings. As suggested by this observation, the pore size distribution in SPS coatings could be modified by adapting the process parameters.

In order to characterize the nano/submicro pores, USAXS measurement were carried out on the nine SPS coatings (S1~S9, see Table 2). The detected pore size distributions of the as-prepared coatings are showed in Fig.4. The content of these pores in the coatings are calculated by integrating their size distributions over all sizes and are presented in Table 3. It can be seen that the process parameters have a significant influence on the pore size and contents, the nano-submicro pores content varies from 9 to 16% for example.

As can be seen from Fig 4, the as-sprayed coatings have a large quantity of pores with the size smaller than 100 nm. Several techniques have been proposed, such as mercury intrusion porosimetry (MIP) [2, 3], x-ray microscopy (XRM) [2], and nuclear magnetic resonance cryoporometry (NMR) [7], to analyze such small pores, but there are still resolution limitations in practical applications. Conversely, the capability of USAXS in measuring very small pore sizes is unprecedented as it is without any limitation of resolution. Moreover, USAXS provides results rapidly if of course the access to synchrotron sources is planed and available for that. It only takes a few minutes to characterize a sample. However, it should be noted that USAXS is not suitable to measure pores over a few micrometer in size. It is the reason why pores larger than 1 μm were ignored and not measured in the current study.

3.2 Multivariate analysis of parameters' influence on the content of nano-submicro pores

In order to investigate the influence of the process parameters on the content of nano-submicro pores, a multivariate analysis was performed by introducing a linear expression of the content *P* of nano-submicro pores:

$$P = c_1*X_1 + c_2*X_2 + c_3*X_3 + c_4*X_4 + c_5*X_5 \quad \text{Eq.2}$$

X_1~X_5 represents the process parameters as defined previously in Table 2 (suspension mass load, powder size, spray distance, spray step, and substrate surface topology, respectively) and c_1~c_5 represent the corresponding correlation coefficients. These correlation coefficients were identified (Table 5) by performing a least square minimization applied to the squared difference *OBJ* between the calculated and the measured porosities, respectively P_i and P_i*:

$$OBJ = \sum_{i=1}^{N}(P_i - P_i^*)^2 \quad \text{Eq.3}$$

N represents the number of samples, which is 9 in the present case.

However, since the process parameters X_1 ~ X_5 of Table 2 present different units and different distribution ranges, a data normalization must therefore be carried out prior to any identification of the correlation coefficients. In this study, a Z-score Normalization is employed [21]:

$$X^* = \frac{X-\overline{X}}{\sigma} \quad ; \quad \overline{X} = \frac{\sum_{i=1}^{5} X_i}{n}; \quad \sigma = \sqrt{\frac{1}{5}\sum_{i=1}^{5}\left(X_i - \overline{X}\right)^2} \quad \text{Eq.4}$$

Where *X* is a vector of 5 lines and 1 row storing the five process parameters, X_i represents the i^{th} component of *X*, $\overline{X}$ is the mean value of *X* and σ its standard deviation. The data matrix after the Z-score Normalization is displayed in Table 4.

The identified correlation coefficients in Table 5 show that the content of nano-submicro pores reduces with the increase of suspension mass load, powder size, and spray step (the slope is negative), while the opposite trend is observed by increasing the others parameters (i.e. the spray distance, or the substrate roughness). Moreover, the content of nano-submicro pores is more sensitive to the suspension mass load that has the largest influence, with a coefficient of 0.555, followed by the powder size (0.487) and the spray distance (0.323), respectively. Finally, the spray step and the substrate roughness have relatively smaller influences, as their coefficients are weak: -0.005 and 0.076, respectively. However, it should be noticed that the coefficient of determination R^2, indicating the efficiency of the identification process, is only equal to 0.83. That means that the identification process is not fully efficient. Consequently, a linear model, such as the one described by Eq.2, does not constitute the best option for predicting properly the dependence of the nano-submicro pores with respect to the process parameters. This is the reason why the next section introduces a predictive model based on a polynomial quadratic expansion.

3.3 Predictive model for the content of nano-submicro pores

In the studied range of parameters, according to the analysis of parameters' influence performed in the previous section, it is possible to identify the role of each process parameter and their influence on the nano-submicro pores. However, a predictive model is necessary for guiding the fabrication of coatings customized for specific applications. If the nano-submicro pores could be predicted from the input process parameters, or if at least some process parameters values could be proposed for manufacturing coatings with customized

nano-submicro pores, it will be highly beneficial from a practical viewpoint. To reach this goal, a purely quadratic polynomial function without cross terms is suggested:

$$P_s = b_0 + \sum_{i=1}^{5} b_i X_i \quad + \sum_{i=1}^{5} b_{ii} X_i^2 \qquad \text{Eq 5}$$

where P_s is the small pores content, X_i represents the process parameters, b_0 is the constant coefficient, b_i and b_{ii} ($1 \leq i \leq 5$) are the linear and quadratic coefficients, respectively.

After applying a Response Surface Methodology [22, 23] for matching the measured small pores content with the quadratic model, Eq 5 can be rewritten by including the identified coefficients:

$$P_s = 5.722 - 1.312 * X_1 + 51.223 * X_2 + 1.027 * X_3 - 1.192 * X_4 - 1.489 * X_5$$

$$+ 0.026 * (X_1)^2 - 156.378 * (X_2)^2 - 0.008 * (X_3)^2 + 0.059 * (X_4)^2 + 0.361 * (X_5)^2 \qquad \text{Eq 6}$$

It should be noticed that the coefficient of determination R^2 indicating the efficiency of the identification process is now equal to 1, which is a perfect value. That proves that it is not useful to use a polynomial of a higher degree than 2 and that quadratic cross terms are neither useful. Figure 5 shows the comparison of experimental data and calculated values based on Eq.2 (for linear model) and Eq.6 (for quadratic model). As expected, because the coefficient of determination is one, the quadratic model matches the experimental results with higher precision than the linear mode meaning thereby that the quadratic model is more efficient for the prediction of nano-submicro pores.

3.4 Evaluation of the predictive model

In order to evaluate the predictive model described by Eq.6, two new coatings (E1 and E2) not considered by the identification process were manufactured with the process parameters listed in Table 6. The USAXS results show the content of small pores equal to 12.24% for coating E1, and 14.76% for coating E2 providing a relative error of 2.94% for coating E1 and 4.53% for coating E2, respectively. That relative error is quite low and is rather acceptable to valid such predictive model. To confirm the relevance of this validation and the correct coefficients of Eq.6, the calculation was done with all the coating (S1~S9, E1 and E2). That reveals a mean relative error of 4.9% compared to 5.8% obtained from Eq.2 (the linear model), corroborating that the quadratic model is more efficient for guiding the coating fabrication.

3.5 Nano-submicro pores tailoring by using the predictive model

In the considered operating window, two approaches can be used to control the nano-submicro pores content in SPS coatings: i) when all process parameters are known, the content can be quickly estimated according to Eq 6. ii) if a specific coating with a given content of such pores is required, the corresponding input process parameters can be determined by using the predictive model. To do that, the 2D distribution of the nano-submicro pores content can be represented as a function of the process parameters as shown in Fig 6, 7 and 8, and the parameter values of interest can be deduced graphically. Detailed explanations are given for Fig 6 displaying the distribution curve of the nano-submicro pores content as a function of the suspension mass load and the powder size (the other process parameters are fixed, spray distance: 40 mm, spray step: 6 mm, substrate roughness: 3.51 µm). If the desired nano-submicro pores content lies in the range between 18.29 and 19.79% (orange color in Fig

6), the mass load must be selected between 11 and 13 wt.% while the powder size must be chosen between about 0.26 and 0.3 µm. In the same manner, Figures 7 and 8 present the distribution of nano-submicro pores content with respect of the suspension mass load and the spray distance for Fig 7, and the powder size and the spray distance for Fig 8, respectively. It is noticed that the isovalues in Fig 8 adopt a remarkable circular shape, contrarily to the isovalues of Fig 6 and 7. This remarkable geometric property comes from the two quadratic terms in Eq 6 related to the powder size X_2 and the spray distance X_3. The coefficients related to these two terms (-156.378 and -0.008, respectively) have indeed the same sign, leading to an ellipsoidal shape. Actually, by reporting the values of the fixed parameters inside the right side of Eq 6, and by reorganizing the terms depending on X_2 and X_3 in the left side, we obtain:

$$156.378 \times (X_2 - 0.164)^2 + 0.008 \times (X_3 - 64.187)^2 = 20.191 - P_s \qquad \text{Eq 7}$$

Eq 7 represents the equation of an ellipse of center $(X_2 = 0.164;\ X_3 = 64.187)$. Note that the location of this center is consistent with the isovalues plotted in Fig 8. Also, note in Fig 8 that these isovalues appear as circle, instead of ellipse, because the unit scales of the horizontal and vertical axis were adapted for a better visualization of the data. Otherwise, the ellipses will appear too much flat.

Contrarily to Fig 8, the isovalues of Fig 6 and 7 exhibit the shape of hyperbolic functions. Eq 6 confirms this visual feeling. Actually, the terms X_1 and X_2 used to plot the isovalues of Fig 6 are associated with the quadratic coefficients of 0.026 and -156.378 in opposite sign. By reporting the values of the fixed parameters inside the right hand side of Eq 6, and by reorganizing the terms depending on X_1 and X_2 in the left hand side, we obtain:

$$0.026 \times (X_1 - 25.231)^2 - 156.378 \times (X_2 - 0.164)^2 = P_s - 15.509 \qquad \text{Eq 8}$$

The minus sign between the two squared terms in Eq 8 allows to recognize the equation of a hyperbolic curve, compared to the plus sign in Eq 7 which is related to the ellipse equation. The coordinates of the corresponding center are: $X_1 = 25.231, X_2 = 0.164$. Note that the location of this center is consistent with the isovalues plotted in Fig 6. A similar conclusion can be drawn from Fig 7 because: 1) the horizontal and vertical axis represent the process parameters X_1 and X_3, 2) the quadratic coefficients related to these two parameters have again an opposite sign in Eq. 6 (0.026 and -0.008, respectively). Considering the terms of Eq 6, the following conclusion can be done on the shape of the porosity distribution, either ellipsoidal or hyperbolic. The porosity distribution depends on the sign of the quadratic coefficients, that is to say either the same sign for an ellipsoidal shape distribution or the opposite sign for an hyperbolic shape distribution.

Fig 9 presents the 3D representation of the content of nano-submicro pores through simultaneously three process parameters. In this figure, the three most influential parameters of the spray process, according to the sensitivity analysis performed in section 3.2, are taken into consideration: spray distance, suspension mass load and powder size. In order to manufacture a coating with a given content, it is sufficient to identify the color corresponding to the desired content in Fig 9, and to select the related set of process parameters. Note that this set is not unique and that several combinations are possible. For example, if a content of 25% is wanted (blue color), seven different combinations of process parameters are possible.

It is also possible to control the nano-submicro pores up to five parameters, the maximum of the current study. However, beyond three parameters, the graphical representations presented previously are no longer suitable. Nevertheless, in such a situation, it could be still possible to link Eq 6 with an optimization algorithm, in order to calculate the process parameters with a numerical scheme. These process parameters would be identified in order to minimize the difference between the numerical prediction of the porosity content (calculated by using Eq 6) and the experimental data. Such an optimization process, involving more than three process parameters, could be developed in further works.

3.6 In-situ observation of sintering effect on nano-submicro pores

In order to observe the sintering effect on the evolution of nano-submicro pores, two samples (coatings S4, S9, see Table 2) were chosen to be sintered at 1200 °C in air over 12 hours and detected in site using USAXS. Figures 10 and 11 show the evolution of nano-submicro pores in coatings as a function of sintering time. The color starts with blue graph at the beginning of the sintering and with red graph at the end of it, crossing in between green and yellow graphs. It can be seen that the pores volume distributions were affected by sintering time. Coating S4 presents significant loss in number with sintering time for the smaller pores less than 200 nm. On the opposite, sintering time has little effect on larger pores bigger than 200 nm. A similar pattern is observed for the coating S9, in which the larger pores seem to be independent of time and the smaller pores present a significant decrease. This observation agrees with the

finding reported by Ekberg et al [8], which showed that many of the smaller pores disappeared after 200 h of heat treatment at 1150 °C. The reason of the change is most probably due to particles agglomeration or pores collapsing during the thermal treatment. Nevertheless, this point needs to be more deeply investigated and questioned in further studied.

Furthermore, comparing with other traditional methods [2-6], which typically need to remove samples from the high temperature environment before the observation of their microstructure, the current work confirmed that USAXS is a time-saving and effective technique for in-situ observation of the finely structure in SPS coatings.

4 Conclusions

USAXS technique was successfully used to detect the nano-submicro pores in SPS coatings. The results demonstrated that the content of nano-submicro pores in SPS coating is influenced significantly by the process parameters. The main results are summarized as follows:

1) USAXS is an effective method for characterizing nano-submicro pores in SPS coatings. The content of nano-submicro pores has a negative correlation with the suspension mass load and the powder size, and a positive correlation with the spray distance, spray step, and substrate roughness.

2) Suspension mass load is the main factor affecting the nano-submicro pores, followed by powder size, spray distance, substrate surface roughness, and spray step, respectively.

3) In the studied operating window, the nano-submicro pores content of SPS coating can be well predicted by a quadratic model, which contains the five input process parameters. Possible parameters could be calculated using the quadratic model for preparing the coating with a given nano-submicro pores content.

The future prospects concern two points:

1) If the number of process parameters is greater than three, it would be necessary to link Eq 6 with an optimization algorithm in order to identify the process parameters giving a desired content of nano-submicro pores.

2) This paper highlights the fact that the coatings present significant change with sintering time for the smaller pores while sintering time has little effect for larger pores (Figures 10 and 11). We have assumed that this decrease of the smallest pores is due to particles agglomeration or pores collapsing during the thermal treatment. Nevertheless, this assumption has to be confirmed by additional experimental observations.

Acknowledgments

This research used resources of the Advanced Photon Source, a U.S. Department of Energy (DOE) Office of Science User Facility operated for the DOE Office of Science by Argonne National Laboratory under Contract No. DE-AC02-06CH11357. This research was also supported by startup research foundation of Shanghai University of Engineering Science No. 201980.

References

[1] Armelle Vardelle, C.M., Jun Akedo et al, *The 2016 Thermal Spray Roadmap.* Journal of Thermal Spray Technology, 2016. **25**(3): p. 1376-1440.

[2] Klement, U., J. Ekberg, and S.T. Kelly, *3D Analysis of Porosity in a Ceramic Coating Using X-ray Microscopy.* Journal of Thermal Spray Technology, 2017. **26**(3): p. 456-463.

[3] Bacciochini, A., et al., *Quantification of void network architectures of suspension plasma-sprayed (SPS) yttria-stabilized zirconia (YSZ) coatings using Ultra-small-angle X-ray scattering (USAXS).* Materials Science and Engineering: A, 2010. **528**(1): p. 91-102.

[4] Zhao, Y., et al., *Experiments, Statistical Analysis, and Modeling to Evaluate the Porosity Influence in SPS Coatings.* Journal of Thermal Spray Technology, 2019. **28**: p. 76-86.

[5] Bacciochini, A., et al., *Quantification of void networks of as-sprayed and annealed nanostructured yttria-stabilized zirconia (YSZ) deposits manufactured by suspension plasma spraying.* Surface and Coatings Technology, 2010. **205**(3): p. 683-689.

[6] Fauchais, P. and A. Vardelle, *Solution and suspension plasma spraying of nanostructure coatings*, in *Advanced Plasma Spray Applications*. 2012, InTech.

[7] Ekberg, J., L. Nordstierna, and U. Klement, *Porosity investigation of yttria-stabilized zirconia topcoats using NMR cryoporometry.* Surface and Coatings Technology, 2017. **315**: p. 468-474.

[8] Ekberg, J., et al., *The Influence of Heat Treatments on the Porosity of Suspension Plasma-Sprayed Yttria-Stabilized Zirconia Coatings.* Journal of Thermal Spray Technology, 2018.

[9] Zhao, Y., et al., *Influence of Substrate Properties on the Formation of Suspension Plasma Sprayed Coatings.* Journal of Thermal Spray Technology, 2018. **27**(1): p. 73-83.

[10] Pawlowski, L., *Suspension and solution thermal spray coatings.* Surface and Coatings Technology, 2009. **203**(19): p. 2807-2829.

[11] Fauchais, P., et al., *Operating parameters for suspension and solution plasma-spray coatings.* Surface and Coatings Technology, 2008. **202**(18): p. 4309-4317.

[12] Tesar, T., et al., *Development of suspension plasma sprayed alumina coatings with high enthalpy plasma torch.* Surface and Coatings Technology, 2017. **325**(Supplement C): p. 277-288.

[13] Sokołowski, P., et al., *The microstructural studies of suspension plasma sprayed zirconia coatings with the use of high-energy plasma torches.* Surface and Coatings Technology, 2017. **318**: p. 250-261.

[14] Ilavsky, J., et al., *Ultra-small-angle X-ray scattering at the Advanced Photon Source.* Journal of Applied Crystallography, 2009. **42**(3): p. 469-479.

[15] Ilavsky, J., et al., *Ultra-Small-Angle X-ray Scattering Instrument at the Advanced Photon Source: History, Recent Development, and Current Status.* Metallurgical and Materials Transactions A, 2013. **44**(1): p. 68-76.

[16] Ilavsky, J., et al., *Development of combined microstructure and structure characterization facility for in situ and operando studies at the Advanced Photon Source.* Journal of Applied Crystallography, 2018. **51**(3): p. 867-882.

[17] Kishitake, K., H. Era, and F. Otsubo, *Characterization of plasma sprayed Fe-17Cr-38Mo-4C amorphous coatings crystallizing at extremely high temperature.* Journal of Thermal Spray Technology, 1996. **5**(3): p. 283-288.

[18] Ilavsky, J. and P.R. Jemian, *Irena: tool suite for modeling and analysis of small-angle scattering.* Journal of Applied Crystallography, 2009. **42**(2): p. 347-353.

[19] Bacciochini, A., et al., *Porous Architecture of SPS Thick YSZ Coatings Structured at the Nanometer Scale (~50 nm).* Journal of Thermal Spray Technology, 2010. **19**(1): p. 198-206.

[20] Tingaud, O., et al., *Suspension plasma-sprayed alumina coating structures: operating parameters versus coating architecture.* Journal of Thermal Spray Technology, 2008. **17**(5-6): p. 662-670.

[21] Celko, J., *9 - Normalization*, in *Joe Celko's SQL for Smarties (Fourth Edition)*. 2011, Morgan Kaufmann: Boston. p. 181-214.

[22] Bezerra, M.A., et al., *Response surface methodology (RSM) as a tool for optimization in analytical chemistry.* Talanta, 2008. **76**(5): p. 965-977.

[23] Pierlot, C., et al., *Design of experiments in thermal spraying: A review.* Surface and Coatings Technology, 2008. **202**(18): p. 4483-4490.

Figure Captions

Fig.1 Particle size distribution of YSZ powders

Fig.2 Schematic of the SPS process and the twin-fluid atomizer

Fig.3 SEM images of as prepared SPS coating (a) top surface (b) cross-section

Fig.4 Volume distribution of nano-submicro pores in as-prepared SPS coating characterized using USAXS

Fig 5 Comparison of experimental data and calculated values using the quadratic model Eq 6

Fig 6 Distribution curve of nano-submicro pores content as a function of suspension mass load and powder size (spray distance: 40 mm, spray step: 6 mm, substrate roughness: 3.15 μm)

Fig 7 Distribution curve of nano-submicro pores content as a function of suspension mass load and spray distance (powder size: 0.36 μm, spray step: 6 mm, substrate roughness: 3.15 μm)

Fig 8 Distribution curve of nano-submicro pore contents as a function of powder size and spray distance (suspension mass load: 25 wt.%, spray step: 6 mm, substrate roughness: 3.15 μm)

Fig 9 Scattering plot of nano-submicro pores content as a function of spray distance, suspension mass load, and powder size (spray step: 6 mm, substrate roughness: 3.15 μm)

Fig 10 Evolution of nano-submicro pores within coating S4 as a function of sintering time

Fig 11 Evolution of nano-submicro pores within coating S9 as a function of sintering time

Tables

Table 1 Process parameters fixed during coating deposition

Parameter	Value
Plasma	Ar: 50 L/min
	H_2: 10 L/min
Suspension flow rate	45 g/min
Spray condition	Line speed: 1000 mm/s
Substrate	304L steel
	Preheating: 300 □
Cooling	Compressed air: 5 Bar

Table 2 Process parameters of the experimental runs and coating characteristic

Sample No.	Mass load: X_1 (wt.%)	Powder size: X_2 (μm)	Spray distance: X_3 (mm)	Spray step: X_4 (mm)	Substrate roughness: X_5 (μm)	Coating thickness (μm)
S1	25	0.36	40	6	0.04	349
S2	25	0.36	40	6	0.16	331
S3	25	0.36	40	6	3.51	338
S4	10	0.36	40	6	3.51	149
S5	25	0.36	70	6	3.51	177
S6	20	0.36	40	3	3.51	251
S7	25	0.36	50	12	3.51	230
S8	20	0.1	40	6	2.45	228
S9	25	0.23	40	6	2.45	235

Table 3 Content of nano-submicro pores in SPS coatings

Sample No.	Pores content (pore size < 1 μm) (%)
S1	10.31
S2	10.14
S3	9.59
S4	15.56
S5	13.42
S6	12.27
S7	11.69
S8	14.96
S9	14.22

Table 4 Data matrix after Z-score Normalization

Sample No.	Mass load: X_1^*	Powder size: X_2^*	Spray distance: X_3^*	Spray step: X_4^*	Substrate roughness: X_5^*	Nano-submicro pores content
S1	0.548	0.471	-0.438	-0.142	-1.718	-0.977
S2	0.548	0.471	-0.438	-0.142	-1.635	-1.055
S3	0.548	0.471	-0.438	-0.142	0.689	-1.305
S4	-2.411	0.471	-0.438	-0.142	0.689	1.408
S5	0.548	0.471	2.521	-0.142	0.689	0.436
S6	-0.438	0.471	-0.438	-1.421	0.689	-0.089
S7	0.548	0.471	0.548	2.416	0.689	-0.352
S8	-0.438	-2.357	-0.438	-0.142	-0.046	1.134
S9	0.548	-0.943	-0.438	-0.142	-0.046	0.800

Table 5 Identified coefficients of Eq 2

Coefficient	c_1	c_2	c_3	c_4	c_5
Value	-0.555	-0.487	0.323	-0.005	0.076

Table 6 Process parameters of evaluation experiments

Coating No.	Mass load (wt.%)	Powder size (μm)	Spray distance (mm)	Spray step (mm)	Substrate roughness (μm)
E1	20	0.36	50	3	3.51
E2	10	0.36	70	12	0.04

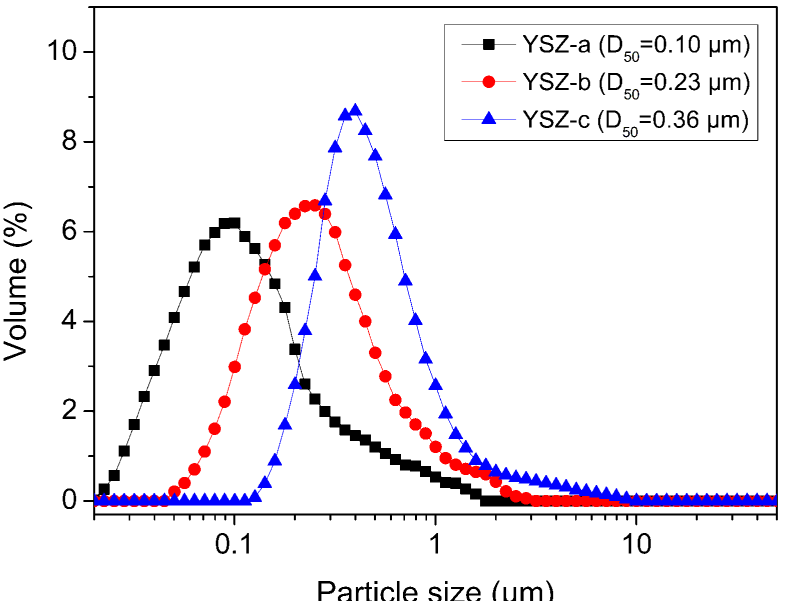
YSZ-a (D_{50}=0.10 μm)
YSZ-b (D_{50}=0.23 μm)
YSZ-c (D_{50}=0.36 μm)
Volume (%)
0
2
4
6
8
10
0.1
1
10
Particle size (μm)

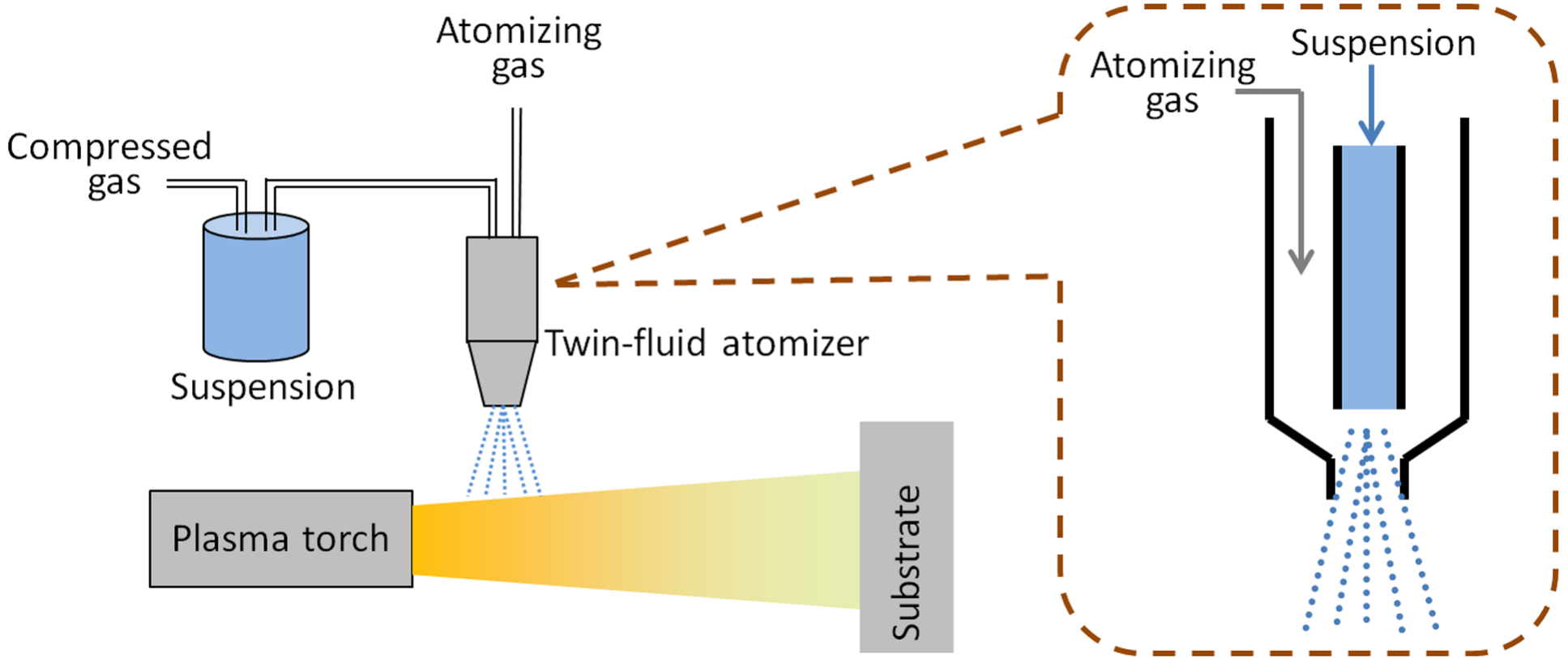
Atomizing gas
Compressed gas
Suspension
Twin-fluid atomizer
Plasma torch
Substrate
Atomizing gas
Suspension

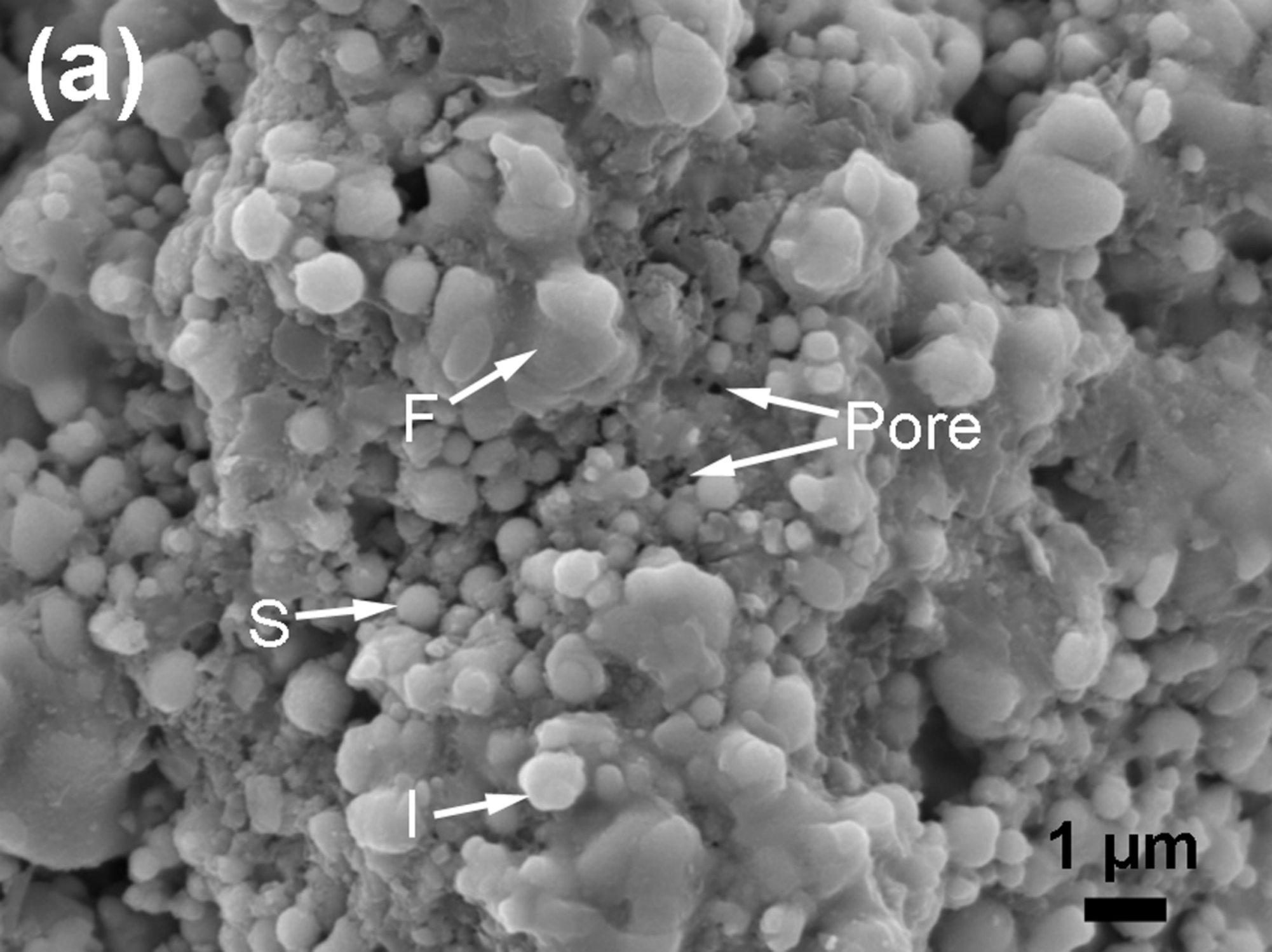
(a)
F
Pore
S
I
1 μm

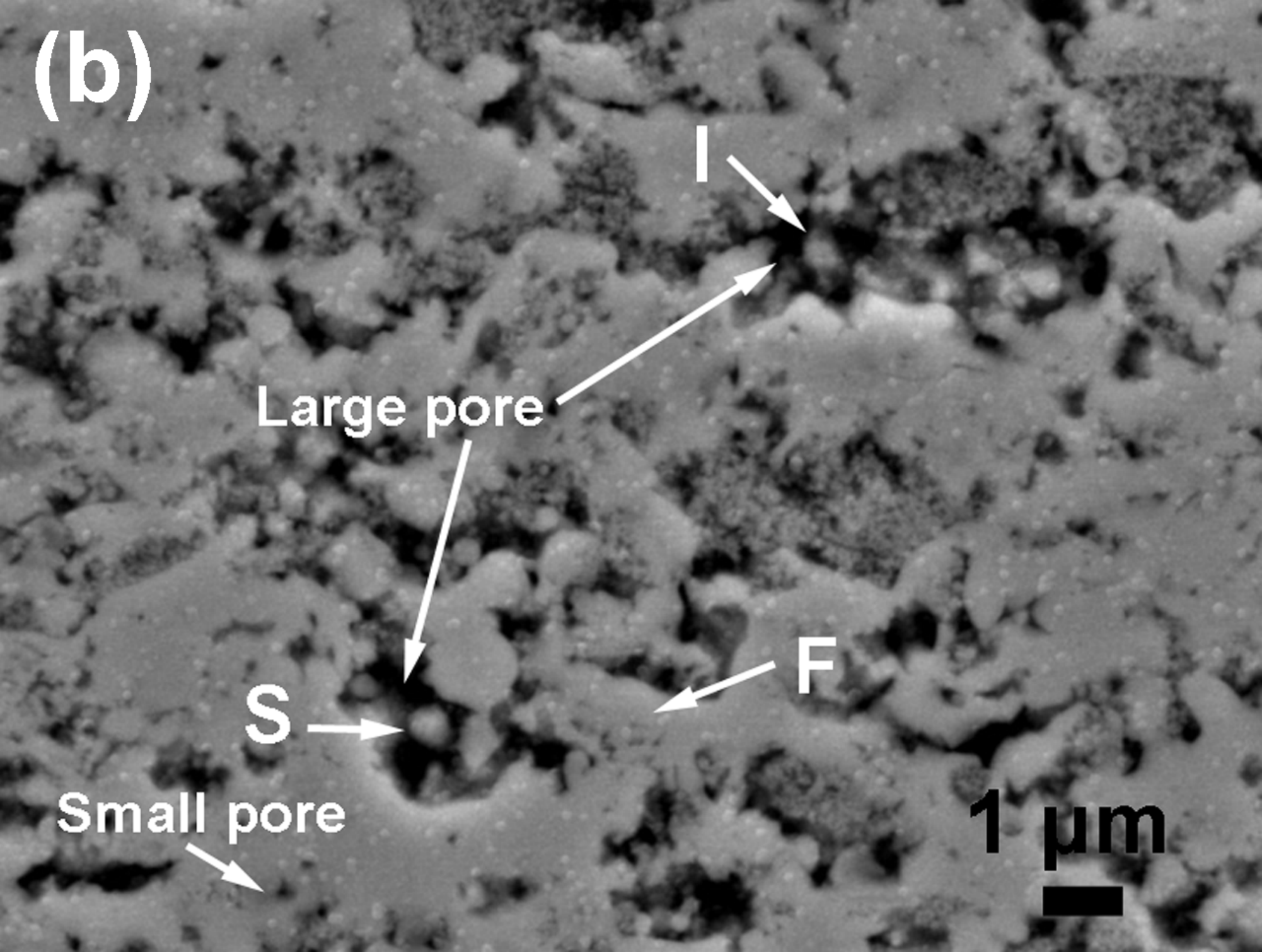
(b)
I
Large pore
F
S
Small pore
1 µm

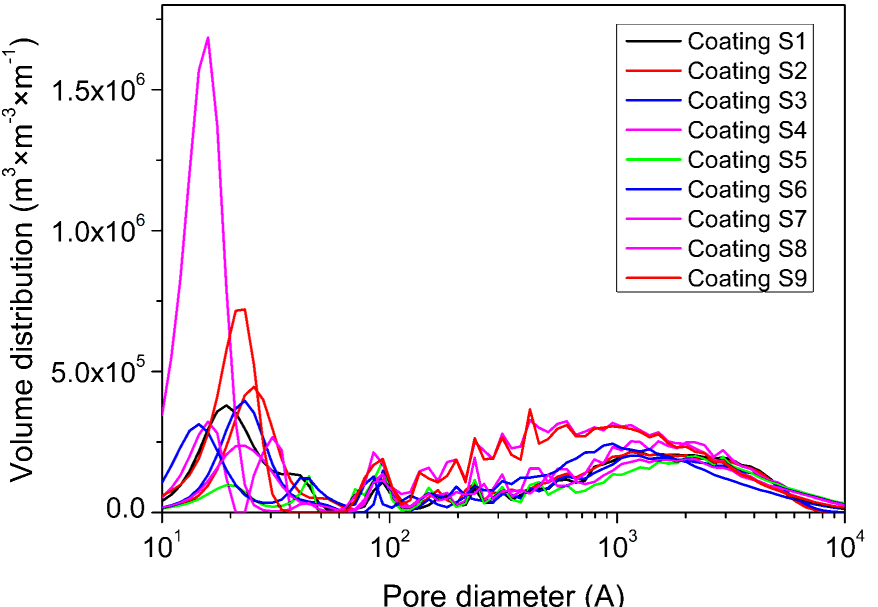
Volume distribution ($m^3 \times m^{-3} \times m^{-1}$)
1.5x10^6
1.0x10^6
5.0x10^5
0.0
10^1
10^2
10^3
10^4
Pore diameter (A)
Coating S1
Coating S2
Coating S3
Coating S4
Coating S5
Coating S6
Coating S7
Coating S8
Coating S9

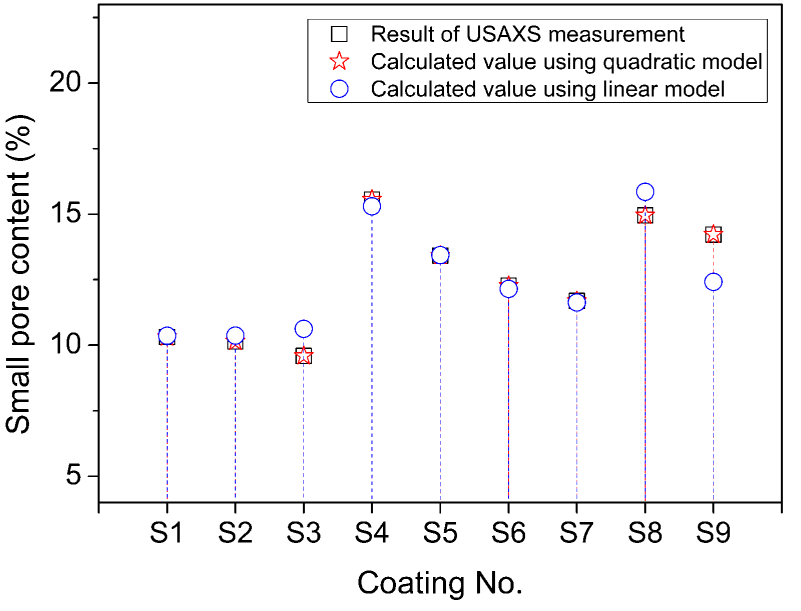
Result of USAXS measurement
Calculated value using quadratic model
Calculated value using linear model
Small pore content (%)
20
15
10
5
S1
S2
S3
S4
S5
S6
S7
S8
S9
Coating No.

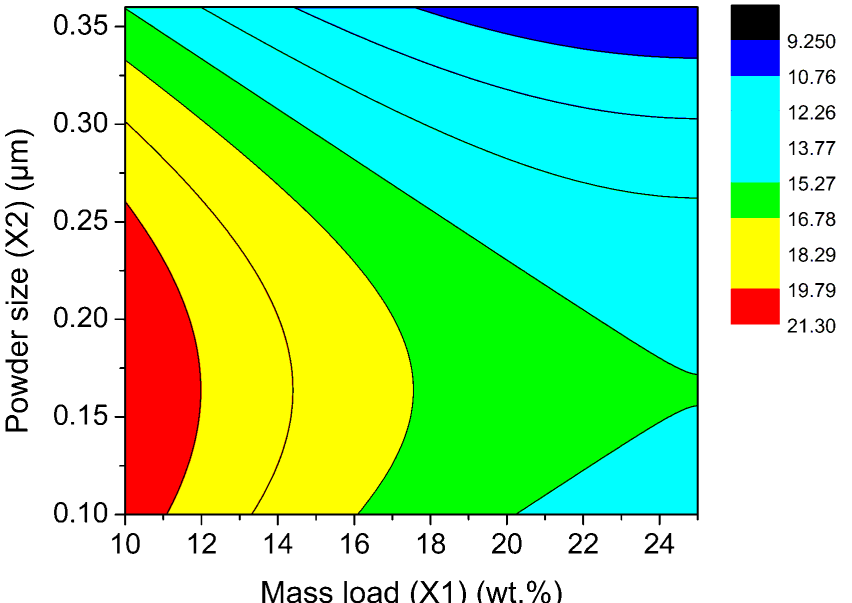
Powder size (X2) (µm)
0.35
0.30
0.25
0.20
0.15
0.10
10
12
14
16
18
20
22
24
Mass load (X1) (wt.%)
9.250
10.76
12.26
13.77
15.27
16.78
18.29
19.79
21.30

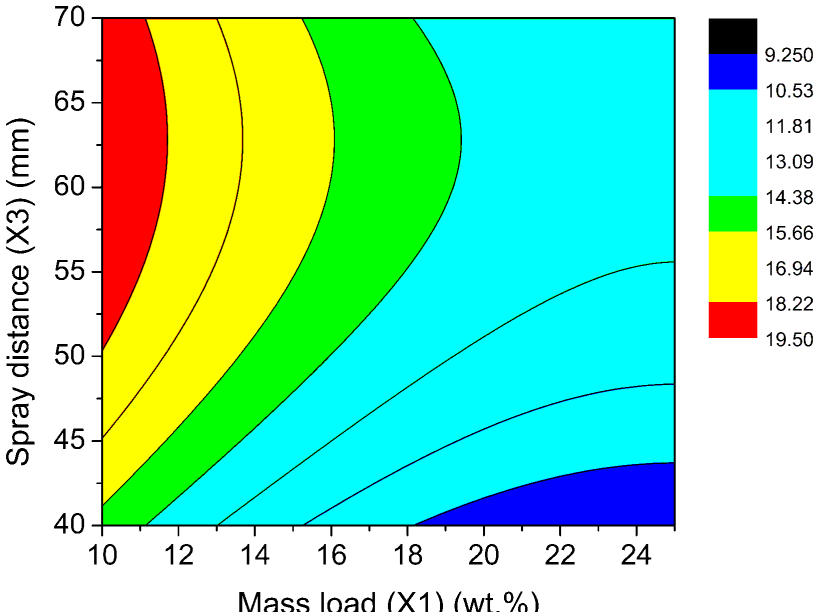
Spray distance (X3) (mm)
70
65
60
55
50
45
40
10
12
14
16
18
20
22
24
Mass load (X1) (wt.%)
9.250
10.53
11.81
13.09
14.38
15.66
16.94
18.22
19.50

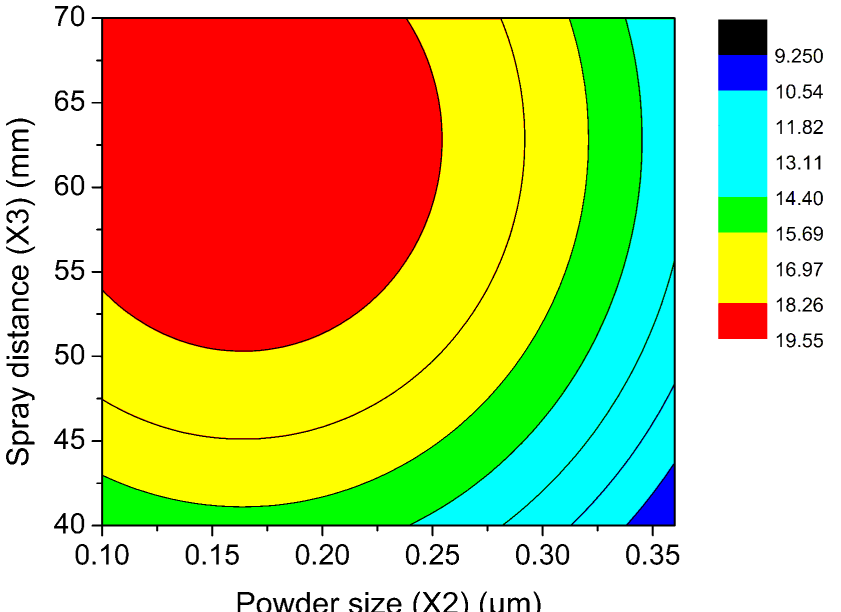
Spray distance (X3) (mm)
70
65
60
55
50
45
40
0.10
0.15
0.20
0.25
0.30
0.35
Powder size (X2) (μm)
9.250
10.54
11.82
13.11
14.40
15.69
16.97
18.26
19.55

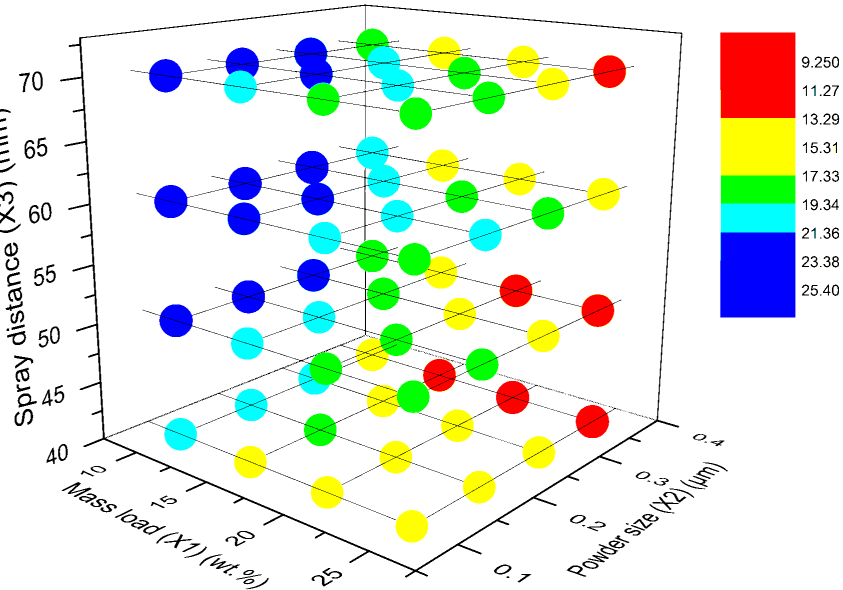
Spray distance (X3) (mm)
70
65
60
55
50
45
40
10
15
20
25
Mass load (X1) (wt.%)
0.1
0.2
0.3
0.4
Powder size (X2) (μm)
9.250
11.27
13.29
15.31
17.33
19.34
21.36
23.38
25.40

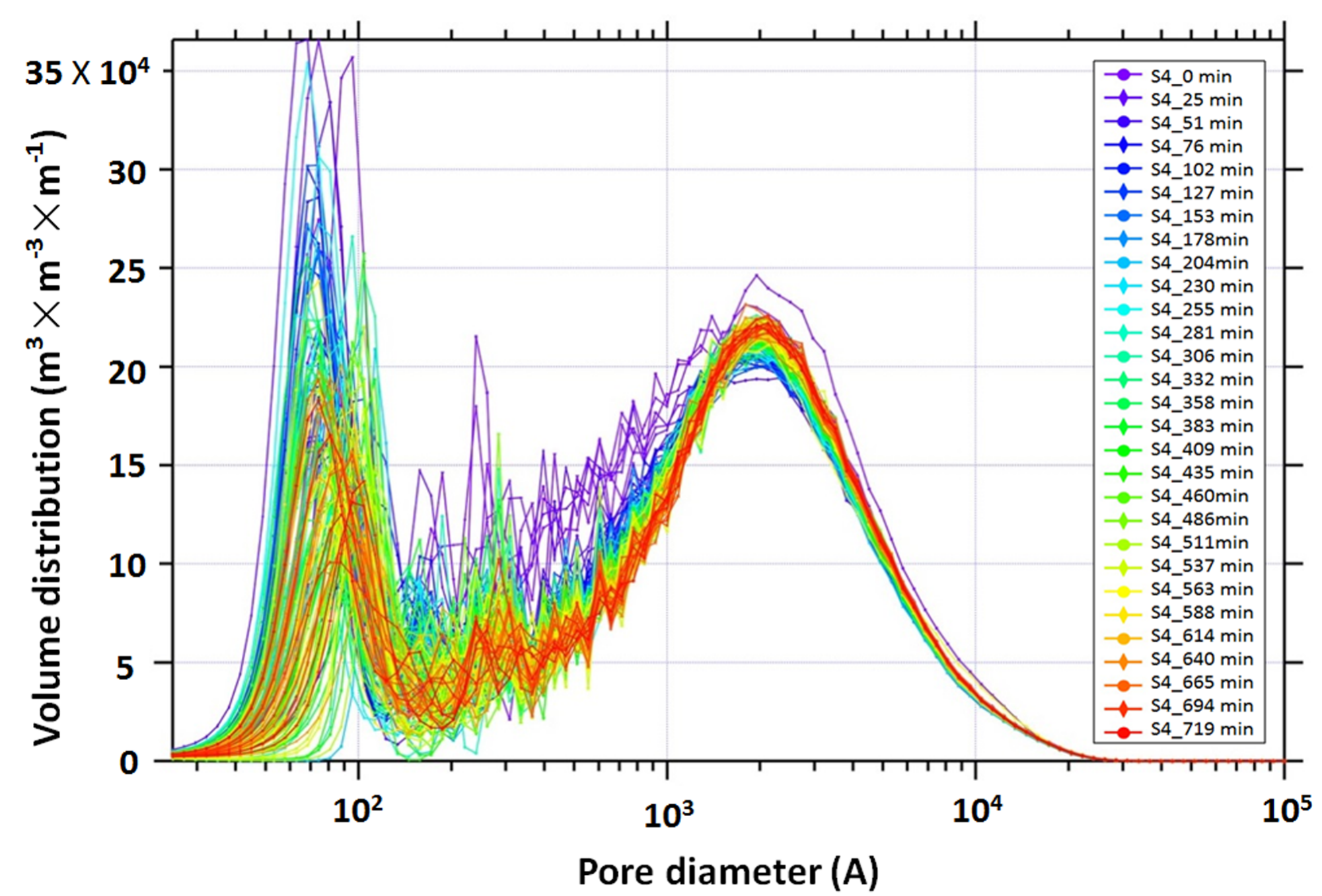
35 X 10^4
30
25
20
15
10
5
0
Volume distribution (m^3 X m^-3 X m^-1)
10^2
10^3
10^4
10^5
Pore diameter (A)
S4_0 min
S4_25 min
S4_51 min
S4_76 min
S4_102 min
S4_127 min
S4_153 min
S4_178min
S4_204min
S4_230 min
S4_255 min
S4_281 min
S4_306 min
S4_332 min
S4_358 min
S4_383 min
S4_409 min
S4_435 min
S4_460min
S4_486min
S4_511min
S4_537 min
S4_563 min
S4_588 min
S4_614 min
S4_640 min
S4_665 min
S4_694 min
S4_719 min

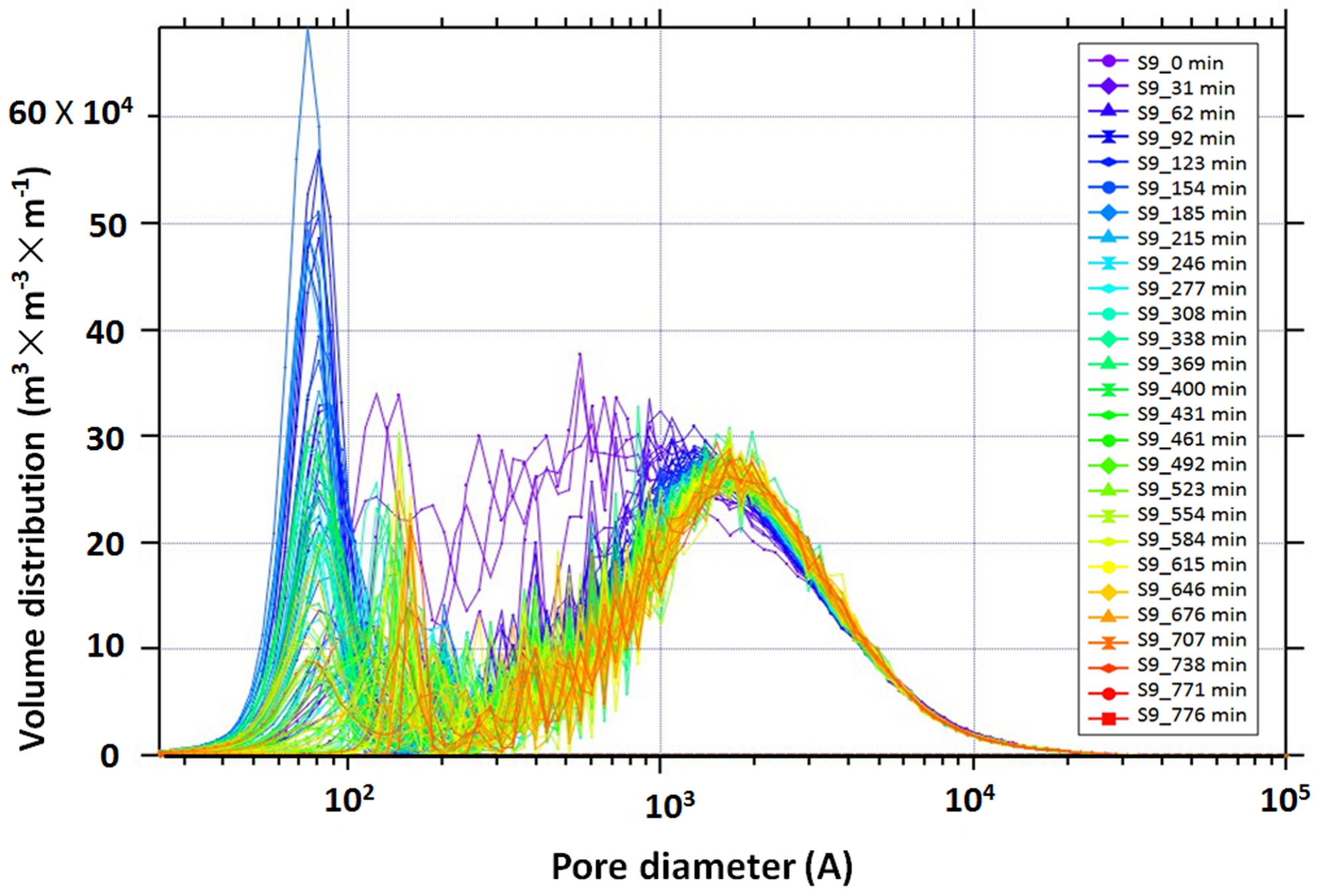
60 X 10^4
50
40
30
20
10
0
Volume distribution (m^3 X m^-3 X m^-1)
10^2
10^3
10^4
10^5
Pore diameter (A)
S9_0 min
S9_31 min
S9_62 min
S9_92 min
S9_123 min
S9_154 min
S9_185 min
S9_215 min
S9_246 min
S9_277 min
S9_308 min
S9_338 min
S9_369 min
S9_400 min
S9_431 min
S9_461 min
S9_492 min
S9_523 min
S9_554 min
S9_584 min
S9_615 min
S9_646 min
S9_676 min
S9_707 min
S9_738 min
S9_771 min
S9_776 min